Scientia Iranica C (2023) 30(6), 2011–2028

Sharif University of Technology
Scientia Iranica
Transactions C: Chemistry and Chemical Engineering
http://scientiairanica.sharif.edu

Comparative study of the X-ray crystallography temperature, synthesis method, optical properties, NCI-RDG, and Hirshfeld surface analyses of coordination polymer of $[Cu^{I}(DAFO)(SCN)]_n$: An amenable precursor for CuO nanoparticles

B. Ramezani[a], G. H. Shahverdizadeh[a,*], L. Edjlali[a], F. Ramezani[b] and M. Babazadeh[a]

a. *Department of Chemistry, Tabriz Branch, Islamic Azad University, Tabriz, Postcode: 5157944533, Iran.*
b. *Department of Molecular Medicine, School of Advanced Medical Sciences, Tabriz, Postcode: 5166653431, Iran.*

Received 26 February 2022; received in revised form 12 December 2022; accepted 30 January 2023

KEYWORDS
Coordination polymer;
X-ray crystallography;
Hirshfeld surface;
Asymmetric unit;
NCI-RDG analysis;
CuO nanoparticles.

Abstract. 1D Coordination Polymer (CP) of $[Cu^{I}(\mu 1,3\text{-NCS})(DAFO)]_n$ (CP1) (DAFO = 4,5-Diazafluoren-9-one) was synthesized using a branched tube method in ethanol and compared with previously synthesized CP2. Although the synthesis methods and parameters for CPs were different, both of them were formed in a similar crystal system (orthorhombic) and space group ($Pmn2_1$) based on their X-ray crystallography data. Optical properties and structure of CP1 were further investigated in detail. Variation of the crystallography temperature causes slight differences in the bond lengths and angles of the geometry center. Hirshfeld surface analyses show the significant contribution of H–C...H (18.9%) for CP1 and H–C...H (19.9%) for CP2. The most obvious distinctions between the CP interactions were C–N (8.4%) and (3.3%), Cu–S (4.8%) and (0.0%), and Cu–N (3.3%) and (11.4%) for CP1 and CP2, respectively. Non-Covalent Interaction-Reduced Density Gradient (NCI-RDG) analysis was conducted to broaden our understanding of the structure-directing interactions in these complexes. CP1 experienced significant inter- and intramolecular interactions according to Hirshfeld surface and NCI-RDG analyses. Solvent-free decomposition of CP1 crystals at 750°C led to the synthesis of copper oxide (CuO) nanoparticles with a particle size of ∼ 12 nm.

1. Introduction

Solid-state crystal structures have evident and secondary effects on chemical properties. Crystal structures determine the arrangement of atoms in a particular material [1]. In addition, they illustrate the length of bond and the value of the lattice parameter of a particular material [2]. Chemical properties originate from atoms of an element making up the material [3]. The primary bonds that hold them together established from the electron configurations of each atom are the main source of chemical properties [4]. Therefore, the atom bonds hold them together and the style of packing

*. *Corresponding authors.*
E-mail addresses: stu.bramazani@iaut.ac.ir (B. Ramezani); shahverdizadeh@iaut.ac.ir (G. H. Shahverdizadeh); l_edjlali@iaut.ac.ir (L. Edjlali); ramezanif@tbzmed.ac.ir (F. Ramezani); babazadeh@iaut.ac.ir (M. Babazadeh)

doi: 10.24200/sci.2023.60012.6558

them determines their properties [5]. Atomic arrangement is responsible for the strength and ductility of the material [6,7].

Recently, the synthesis of copper Coordination Polymers (CPs) has attracted the attention of many scientists [8] because of their perceived potential, fascinating structural properties, and their important applications such as medical, luminescent, magnetic, and catalytic properties, ascribing copper(I) and copper(II) CPs [9–13]. Anions like thiocyanate (SCN^-) and azide (N_3^-) acting as bridging ligands play a prominent role in determining the structure of polymeric metal-organic compounds, particularly when the chelating ligand is neutral. The thiocyanate anion is coordinated either through nitrogen (N) or sulfur (S) atom or both, giving rise to linkage isomers, dimers, or polymers [14].

Metal oxide nanoparticles (NPs), especially copper oxide (CuO) (NPs), are the focus of many scientists because of their versatile applications in various research fields such as medicine, optics, catalysts, and sensors [15,16]. To date, microwave synthesis, solvothermal, sol-gel process, precipitation, and chemical vapor methods represent various synthesis methods developed for preparing metal oxide NPs. However, among them, the thermal decomposition of transition metal coordination complexes to nanoparticles of metal oxide NPs is of high priority due to its facile control of synthesis, crystal structure, NP size, precise choice of precursors, cost-effectiveness, purity, and high yields [8].

In the present study, our primary goal is to synthesize copper coordination with two different bridging ligands of SCN^- and N_3^-. Contrary to our expectation, N_3^- did not enter the geometry center. In our reaction condition, the dominant mechanism might be 2H-tetrazole-5-ammoniumthiolate (Cu-intermediate) formation of $[Cu^I(\mu 1,3\text{-NCS})(DAFO)]_n$ [17,18]. It appears that our synthesis method is a simple cost-effective one compared with the synthesis method proposed by Kulkarni et al. [19]. Based on our crystallography data, the crystal system and space group of our CP were similar to the CP synthesized by Kulkarni et al. The difference between the crystallography temperature obtained by our method (290 K) and that of Kulkarni et al. (200 K) revealed that temperature had a minor effect on the bond length and angles in the crystal environment of a coordination compound. However, the origin of intra- and inter-action bonds may change following temperature variation. The temperature affects the bond length of the S...O intermolecular chalcogen bond and the origin of the $\pi - \pi$ interaction of the SCN^- group with 4,5-Diazafluoren-9-one (DAFO) carbons. Ultraviolet-visible (UV-vis) and Fourier Transform Infrared (FT-IR) spectra confirmed the structure and bonds of our CP1 in the crystal structure. The value of bandgap energy ($E_g = 5.63$ eV) confirmed that CP1 could be classified as a class of ultrawide band-gap energy materials. Differences in C–N, Cu–S, and Cu–N interactions, which were detected based on the 3D Hirshfeld Surface (HS) analysis and 2D Fingerprint Plots (2D FP) of both CPs, result from the difference between our crystallography method and the method suggested by Kulkarni et al. [19] in terms of determining the asymmetric unit. In this highlight, we describe the Non-Covalent Interaction (NCI) computational method and its implementation for the analysis and visualization of weak interactions in the CP1 crystal structure. Our study suggests that it is important to determine appropriate asymmetric units in the course of gathering crystallography data. Also, in this study, thermal decomposition is presented as a facile, solvent-free, and solid-state method for the preparation of pure and relatively small CuO NPs.

2. Materials and methods

2.1. Materials

All reagents and solvents were purchased from commercial vendors and used as received without further purification, except DAFO synthesized by the referenced method in [20].

2.2. Characterization techniques

A suitable crystal of $[Cu^I(DAFO)(SCN)]_n$ was selected and placed on a MAR-345dtb diffractometer (MarXperts German Stifterverband). The crystal was kept at 290.00 K during data collection. Using Olex2 [21], the structure problem was resolved with the help of the SHELXD [22] structure solution program using dual space and refined with the SHELXL [21] refinement package using Gauss-Newton minimization. FT-IR and UV-vis (as pellets with KBr) data were collected using Brucker TENSOR 27 (Bruker Inc., Germany(and Shimadzu UV-1800 (Shimadzu's original LO-RAY-LIGH, Japan), respectively. Crystallexplore 21.5 is the software for analyzing the 3D HS analysis and 2D finger plots of both CPs. The Reduced Density Gradient (RDG), also known as the NCI method, was applied via NCIweb server, which is an online platform accessible through the following link: https://nciweb.dsi.upmc.fr/index.php.

2.3. Synthesis of DAFO ligand

The synthesis of DAFO was carried out via the referenced method [20]. A 350 mL aqueous solution mixture of 1,10-Phenanthroline monohydrate (5 g, 0.0252 mol) and KOH (5 g, 0.088 mol) was heated to 90°C in a 1000 ml round-bottom flask. A hot solution of $KMnO_4$ (12.5 g, 0.079 mol) in H_2O (200 mL) was then added dropwise for 2 hours, followed by constant stirring. Next, the reaction mixture was heated further for 10 min and then, hot-filtered. After removing dark residues of MnO_2, the solution was cooled and its pH was adjusted

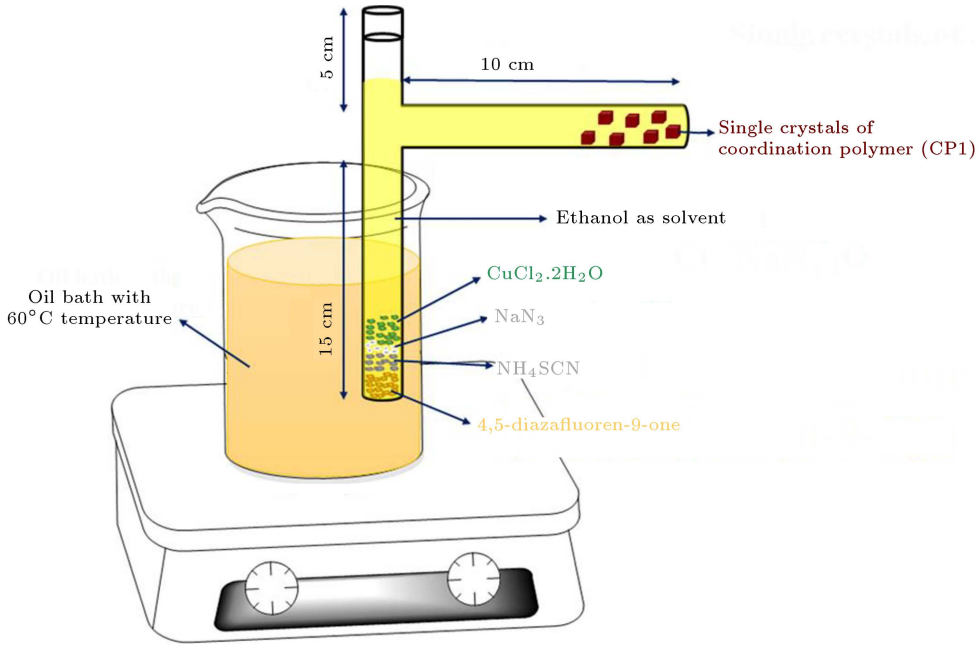

Scheme 1. Graphical abstract for the synthesis of one-dimensional CP of compound (1).

at 9. The resulting orange residues were filtered and washed with cold distilled water (3×50 mL). Moreover, the remaining residues were extracted from the solution with chloroform (3×100 mL). The solvent was removed by a rotary evaporator and then, all of the residues were collected and recrystallized twice from distilled water to give DAFO as pale-yellow crystals.

2.4. General procedure for the synthesis of one-dimensional CP $[Cu(\mu 1,3\text{-}NCS)(DAFO)]_n$ (CP1)

Scheme 1 illustrates the synthesis of single crystals of CP1 using the solvothermal process in ethanol through the branched tube method. DAFO (1 mmol, 0.182 g), ammonium thiocyanate (NH_4SCN) (1 mmol, 0.076 g), sodium azide (NaN_3) (1 mmol, 0.065 g), and copper(II) chloride dihydrate ($CuCl_2.\ 2H_2O$) (2 mmol, 0.34 g) were poured into the bottom of the main arm of a branched tube and then, filled with ethanol. Due to filling ethanol gently into both arms of the branched-tube, the solvent became clear inside both arms of the tube. After sealing the tube, the material-contained arm was placed in oil bath at 60°C, while the other arm was kept at ambient temperature. After 3 days, brown cubic crystals were obtained and then, filtered off and air dried (yield: 84%).

3. Results and discussion

3.1. Comparison of two different synthesis methods of $[Cu^I(\mu 1,3\text{-}NCS)(DAFO)]_n$

Our primary goal is to synthesize a coordination compound with different bridging ligands containing both N_3^- and SCN^- anions with copper as a central metal ion and DAFO as the main ligand. Among the bridging ligands, SCN^- coordinated with Cu(II) might be related to the coordination capacity of SCN^- anion, which is a highly versatile ambidentate and is stronger than N_3^- anion. Therefore, contrary to our expectation, N_3^- anion as a bridging ligand did not enter the coordination geometry center of CP1. Although we are not able to impose synthetic control, an amazing variety of acentric and new CPs have been prepared from hydrothermal reactions. These reactions not only are often quite complicated but also may consist of in-situ oxidation, reduction, hydrolysis, and ligand synthesis. Direct mixing of solutions of ligands and metal salts cannot normally generate metal-organic compounds that form under hydrothermal reaction conditions [17]. The 2H-tetrazole-5-ammoniumthiolate is prepared following the addition of azide to thiocyanate in ethanol with copper (Cu) salts as Lewis acid catalysts (Scheme 2). Although the role of Cu in the reaction is not clear, it can be predicted by the suggested solid intermediate ($(PhCN_4)_2Zn$) in the reaction of PhCN with $ZnBr_2$ and NaN_3 [23]. Identification of our Cu-intermediate may provide a key point to the role of Cu in such reactions. This, in turn, may widen synthetic chemists' board of view for further synthesis of new and fascinating copper-based CPs. It is assumed that our CP1 is synthesized via the suggested mechanism (Cu-intermediate) in Scheme 2 [17,24].

Table 1 shows the essential information of crystal data and structure refinement for our CP1 and CP2 synthesized by Kulkarni et al. with CCDC No. 170071 [19]. The synthesis methods for both CPs were compared and described in the following. CP1 (brown cubic single crystals) was formed via a thermal reaction of

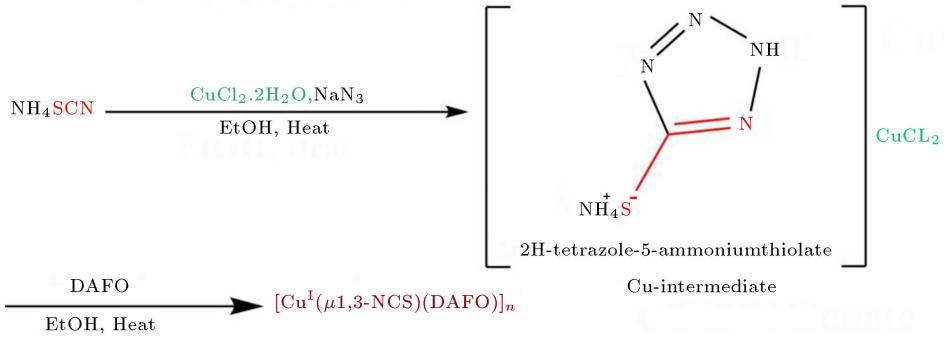

Scheme 2. Suggested reaction mechanism of formation 1D CP of $[Cu^{I}(\mu 1,3\text{-NCS})(DAFO)]_n$ under our reaction condition.

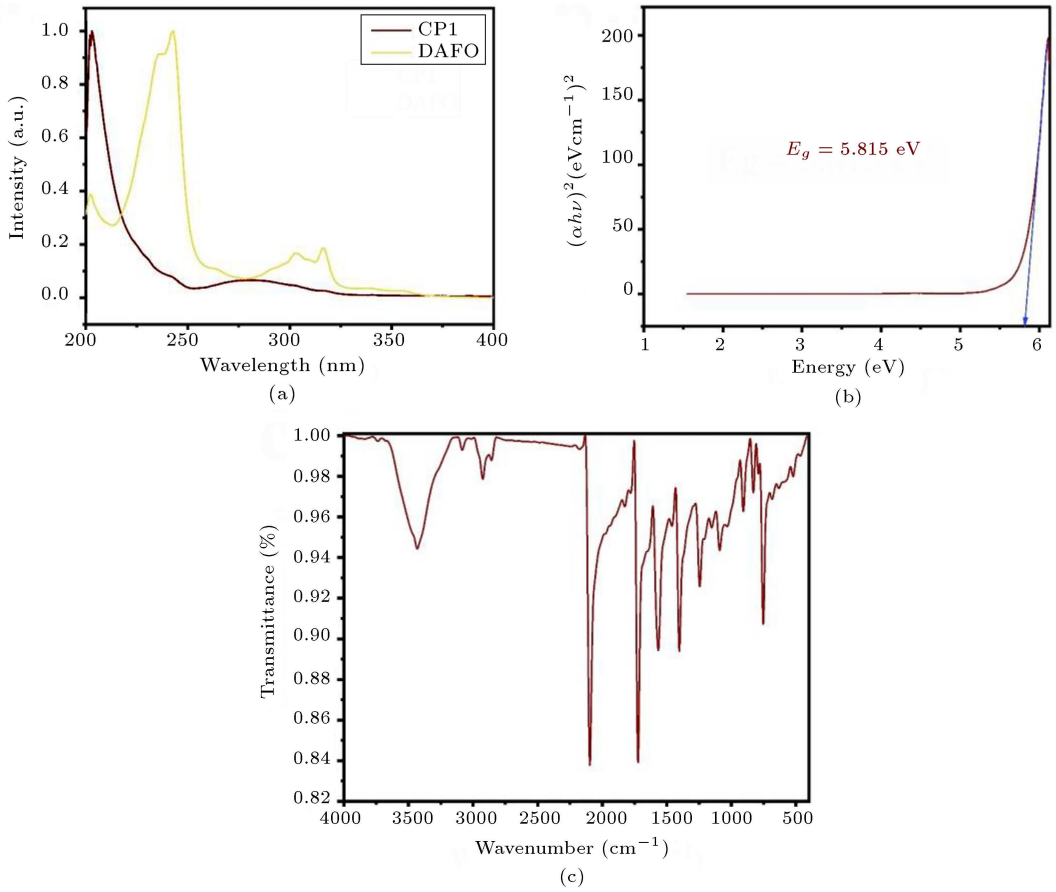

Figure 1. (a) UV-vis spectrum of CP1 in ethanol; (b) Bandgap energy of CP1 at the λ_{max} of UV-vis spectrum; and (c) FT-IR spectrum of CP1.

$CuCl_2.2H_2O$ and DAFO in ethanol in a branch tube (see Scheme 1) at 60°C in the presence of NH_4SCN and NaN_3. In contrast, CP2 (as a bright orange needle-single crystal) was synthesized by Kulkarni et al. in acetonitrile solutions of $Cu^{I}(CH_3CN)_4BF_4$ and DAFO in the presence of four-fold excess of NH_4SCN. Of note, although X-ray single-crystallographic data show that our CP1 structure is similar to CP2 synthesized by Kulkarni et al., we prepared X-ray single-crystallographic data for our CP1 for a better comparison.

3.2. UV-vis and FT-IR spectra and bandgap energy of $[Cu^{I}(\mu 1,3\text{-NCS})(DAFO)]_n$ (CP1)

CP1 is slightly dissolved in warm ethanol because copper(I) thiocyanates coordination compounds are extremely insoluble in common solvents [18]. Since the electron-donating ability of the DAFO ligand is weak, the transition exhibits a high-energy transition near ultraviolet [25,26]. In the UV spectra (Figure 1(a)), the bands in wavelengths 205 and 208 nm in CP1 and 236 and 243 in DAFO could be assigned to

Table 1. Crystal data and structural refinement parameters for **CP1** and **CP2**.

Compound name	**CP1**	**CP2**
Chemical formula	$C_{12}H_6CuN_3OS$	$C_{12}H_6CuN_3OS$
M_r	303.80	303.80
Crystal system, space group	Orthorhombic, $Pmn2_1$	Orthorhombic, $Pmn2_1$
Temperature (K)	290	200
a, b, c (Å)	12.826 (3), 5.7032 (11), 7.8840 (16)	12.666 (7), 5.690 (3), 7.743 (4)
V (Å^3)	576.7 (2)	558.1 (6)
Z	2	2
Radiation type	Mo $K\alpha$	Mo $K\alpha$
μ (mm^{-1})	2.06	2.13
Crystal size (mm)	0.15 × 0.1 × 0.1	0.25 × 0.15 × 0.05
Diffractometer	MAR-345dtb	Bruker *SMART* Apex
Absorption correction	–	Empirical (using intensity measurements) SADABS (Bruker AXS Inc., 2000)
No. of measured, independent and observed $[I > 2\sigma(I)]$ reflections	3826, 1176, 1101	3206, 1265, 1158
R_{int}	0.047	0.048
$(\sin\theta/\lambda)_{\max}$ (Å^{-1})	0.624	0.659
$R[F^2 > 2\sigma(F^2)]$, $wR(F^2), S$	0.046, 0.115, 1.11	0.049, 0.133, 1.15
No. of reflections	1176	1265
No. of parameters	104	93
No. of restraints	11	1
H-atom treatment	All H-atom parameters refined	H atoms treated by a mixture of independent and constrained refinement
$\Delta\rho_{\max}$, $\Delta\rho_{\min}$ (e Å^{-3})	0.38, –0.49	0.46, –0.58
Absolute structure	Refined as an inversion twin.	Flack H D (1983), Acta Cryst. A39, 876–881
Absolute structure parameter	0.11 (5)	0.13 (3)

the ligand-centered $\pi \rightarrow \pi^*$ excitation transitions of the aromatic rings [26,27]. These bands are sensitive to substitution at aromatic rings [20,28]. This band shows a blue shift with $\sim$ 30 nm in the spectrum of CP1, confirming the covalently binding of ligand to copper metal center [25,26,28]. The absorption wavelengths at 248 and 277 nm in CP1 (264 and 303 nm in DAFO) UV-vis spectrum might be attributed to the intra-ligand $n \rightarrow \pi^*$ transition of C=N and C=C bonds and conjugated aromatic chromophore [20,26]. The $n \rightarrow \pi^*$ characteristic wide band assigned to the C=O bond appears at 278 nm in the CP1 spectrum

(317 nm for DAFO). With a 50 nm blue shift and its widening, the presence of a ligand in the complex and the presence of S...O intermolecular chalcogen bonds can be proven. Because the chalcogen-bonding intermolecular interactions in CP1 are dominated by $n \rightarrow \sigma^*$ orbital delocalization between a lone pair of $O_{(C=O)}$ donor and the antibonding σ^* orbital of an acceptor $S_{(SCN)}$, it might improve electronic communication between neighboring CP1 moieties in the infinite columnar assembly without relying on $\pi - \pi$ interactions [29]. The hypsochromic shift indicates that the ground state is more sensitive than the excited state, as the excited state structure has a lower dipole moment than the ground state. Due to the donor ability of C_2H_5OH as a polar protic solvent, ground state π is expected to be less stable than state π^* excited. Ethanol ability to form a hydrogen bond donator seems to stabilize the excited state of the electronic transitions via solute-solvent interactions [28–30]. The optical bandgap energy using the absorption edge of the UV-vis spectra (λ_{max}) of single crystals of CP1 was calculated according to the Tauc Plot and its value is $E_g = 5.63$ eV (Figure 1(b)) [20]. The value of E_g can classify our CP1 as an ultrawide-bandgap (3.4–6.0 eV) semiconductor material [31].

As can be seen in Figure 1(c), the FT-IR spectrum of CP1 shows a strong absorption at 3475 cm^{-1}, which might be originated from the whole O...H interaction in the crystal packing system. Aromatic C–H stretching frequency can be observed at 3078 and 3010 cm^{-1}. The asymmetric and symmetric stretching vibrations of the carbonyl group (C=O) appear at 1650 cm^{-1} and 1380 cm^{-1}, respectively [26]. Due to the intermolecular S...O chalcogen bonds between the oxygen of the carbonyl group and sulfur in the bridging ligand of the other chain, the stretching vibration of the C=O group demonstrates a shift to a lower wavenumber. The IR spectra show an intense absorption band corresponding to the thiocyanate anion at ν(CN) 2150 cm^{-1}. The C–O of -COOH stretching frequency is stamped at 1120 cm^{-1}. The weak frequencies at 416–615 cm^{-1} can be attributed to ν(Cu–N) and ν(Cu–O).

3.3. Comparing SCX-ray crystallography of CP1 and CP2

CP1 and CP2 are neutral thiocyanato-bridged one-dimensional coordination polymers, as illustrated by single-crystal X-ray diffraction analysis. Both CPs are crystallized in $Pmn2_1$ space group of orthorhombic crystal system. The molecular structure of the CPs is shown in Figure 2, and the selected bond lengths and angles are presented in Table 1.

In both CPs, Cu(I) ion has a distorted tetrahedral coordination environment, which is created by the coordination of two nitrogen atoms from an organic ligand, as well as nitrogen and sulfur atoms of thiocyanate bridging ligand (see Figure 2(a) and (b)). The environment of copper atoms in both CPs $[Cu^{I}(DAFO)(SCN)]_n$ is CuN3S. The μ-$_{1,3}$-SCN bridge connects Cu(I) ions to form a 1D polymeric chain along with b crystallographic axis (see Figure 2(c) and (d)).

The Cu(I)...Cu(I) distance through μ-$_{1,3}$-SCN bridge is 5.703 Å for CP1 and 5.690 Å for CP2. The $N1^{i}$–Cu1–N1 angle (82.7 (3)°) in CP1 and $N2^{ii}$–Cu1–N2 (83.0 (2)°) are the smallest angles around tetrahedral Cu(I) core, which can be attributed to the formation of a five-membered ring by the coordination of two nitrogen atoms from DAFO ligand. The N2–C7–S1 angle (179.4 (8)°) in CP1 and the S1–C1–N1 angle (177.8 (6)°) in CP2 indicate that SCN is almost linear. The Cu–$N_{(thiocyanate)}$ bond length in both CPs is the same. Cu–$N_{(5-membered\ ring)}$ is 2.220 Å (Cu1–N1) in CP1 and 2.196 Å in CP2.

According to the data shown in Table 2, the 5-membered ring in the geometry center in CP1 is slightly larger than that in CP2. The Cu–N and Cu–S bond lengths in both CPs are in the normal range observed for other Cu(I) coordination compounds [19]. There is a strong intermolecular S...O chalcogen interaction between the S atom of the coordinated thiocyanate bridge and the oxygen atom of DAFO ligand from the neighboring polymeric chain in both CPs. This interaction converts the 1D polymeric chain into a 2D polymeric network on the bc plane (see Figure 2(c) and (d)).

Figure 3 reveals that the crystallography temperature has a slight effect on the bond length, but a distinguished effect on the bond origin of inter- and intramolecular interactions. That is, the intermolecular S...O chalcogen interaction in CP1 and CP2 is 3.17 and 3.099 Å, respectively. The difference might lead to the changing of the intramolecular interaction bond length and origin in both CPs.

Figure 3 clearly illustrates the $\pi_{C7ii(C=N)...}\pi_{C(DAFO)}$ interaction with bond length and origin in CP1 and the $\pi_{N1(C=N)...}\pi_{C(DAFO)}$ interaction with bond length and origin in CP2. The difference in the π–π interaction results from crystallography temperature and intermolecular S...O chalcogen bond length.

The π–π interaction changed from $\pi_{C7ii(C=N)...}\pi_{C(DAFO)}$ interaction in CP1 to $\pi_{N1(C=N)...}\pi_{C(DAFO)}$ interaction in CP2 due to the decrease in the bond length of intermolecular S...O chalcogen bond. This apparent change may result from the increase in CP1 crystallographic temperature during the collection of crystallographic data.

3.4. Comparative study on the HS analysis of CP1 and CP2

The HS is characterized by two distances: distances from the surface to the nearest nucleus external (d_e) and internal (d_i) to it. In other words, distances d_e

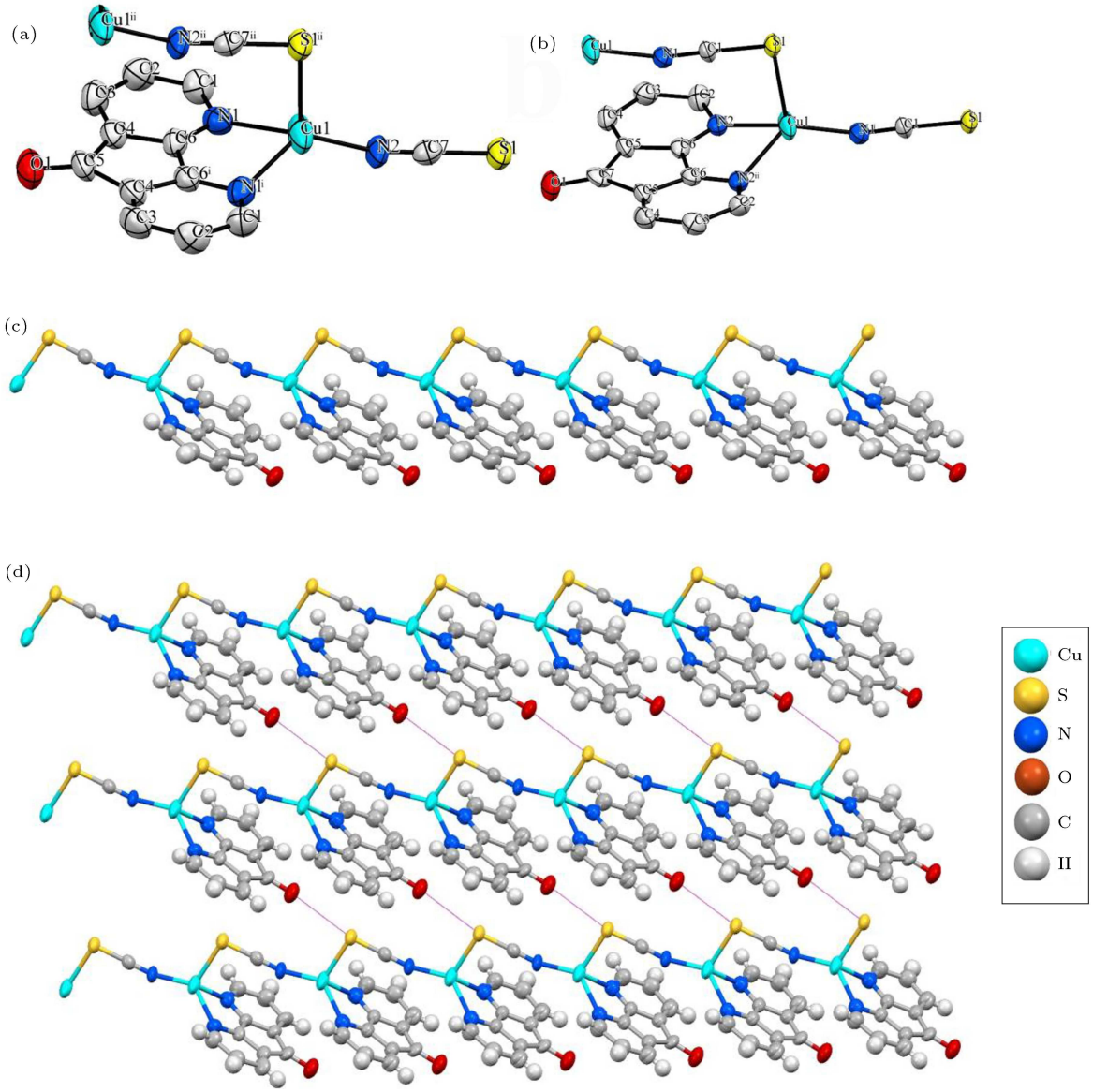

Figure 2. Molecular structure and coordination environment of Cu(I) ion in (a) CP1, (b) CP2; (c)1D polymeric chain obtained by μ-$_{1,3}$-SCN bridge in the crystal structure of CP1,2, (d) 2D polymeric network obtained by intermolecular interactions in the crystal structure of CP1,2.

when color-mapped on the surface visualize close intermolecular interactions, particularly hydrogen bonds, and voids where interactions are the weakest [32]. 2D FP is obtained through the analysis of intermolecular interactions by mapping three-dimensional d_{norm} surfaces with d_i and d_e contact distances from the HS to the nearest atom inside and outside, respectively [24]. Mapping the surface over d_{norm} highlights a variety of red dots that emphasize distances shorter than the sum of the van der Waals (vdW) radii [33,34]. These dominant contacts correspond to the intra-molecular close contact pertaining to Cu–S, Cu–N, $C_{(\text{N-pyridyl moiety})}$–$C_{(\text{5-membered ring})}$, and $C_{(\text{ketone moiety})}$–$C_{(\text{5-membered ring})}$ for CP1 and Cu–N^{i}, Cu–N^{ii}, $C_{(\text{N-pyridyl moiety})}$–$C_{(\text{5-membered ring})}$, and $C_{(\text{ketone moiety})}$–$C_{(\text{5-membered ring})}$ for CP2. Moreover, the strong S...O interaction is an inter-molecular close contact in both CPs (Figure 4(a) and (c)). Figure 4(b) and (d) shows the upper spike distances from the surface to the nearest nucleus external (d_e), while the lower spike demonstrates internal (d_i) distances.

Distinguished pairs of sharp spikes of approximately equal lengths in the area 1.6 Å $< (d_e + d_i) <$ 2.4 Å in the fingerprint plot are characteristics of nearly equal C–C and Cu–X (X = O, N, S) distances for CPs **1** and **2**. Reducing the values of di and de scales of 2DFP of HS analysis from the wing to tale(s) indicates close contact between atoms in the crystal structure (Figure 4(b) and (d)).

According to Figure 5, the $d_e + d_i$ contacts

Table 2. Selected bond length and angles for **CP1** and **CP2**.

CP1		CP2	
Bond	**Length (Å)**	**Bond**	**Length (Å)**
Cu1–S1^{ii}	2.393 (3)	Cu1–S1	2.374 (2)
Cu1–N2	1.882 (8)	Cu1–N1^{i}	1.882 (6)
Cu1–N1	2.220 (6)	Cu1–N2^{ii}	2.196 (4)
Cu1–N1^{i}	2.220 (6)	Cu1–N2	2.196 (4)
S1–C7	1.651 (9)	S1–C1	1.660 (6)
N1–C1	1.344 (9)	N2–C2	1.339 (8)
O1–C5	1.217 (12)	O1–C7	1.236 (10)
N1–C6	1.327 (8)	N2–C6	1.307 (8)
N2–C7	1.150 (11)	N1^{i}–C1	1.137 (6)
Bond	**Angle (°)**	**Bond**	**Angle (°)**
N2–Cu1–S1^{ii}	111.55 (3)	S1–Cu1–N1^{i}	111.95 (19)
N2–Cu1–N1	127.56 (2)	N1^{i}–Cu1–N2	127.21 (15)
N1–Cu1–S1^{ii}	100.54 (15)	S1–Cu1–N^{ii}	100.58 (12)
N1^{i}–Cu1–N1	82.75 (3)	N2–Cu1–N2^{ii}	83.03 (2)
N2–C7–S1	179.4 (8)	S1–C1–N1	177.8 (6)
C7^{ii}–S1^{ii}–Cu1	98.16 (3)	Cu1–S1–C1	98.78 (2)
C7–N2–Cu1	166.0 (8)	C1–N1–Cu1	164.63 (6)

Symmetry codes for CP1: (i) $-x+1$, y, z; (ii) x, $y-1$, z. and
Symmetry codes for CP2: (i) x, $y+1$, z; (ii) $-x$, y, z; (iii) x, $y-1$, z.

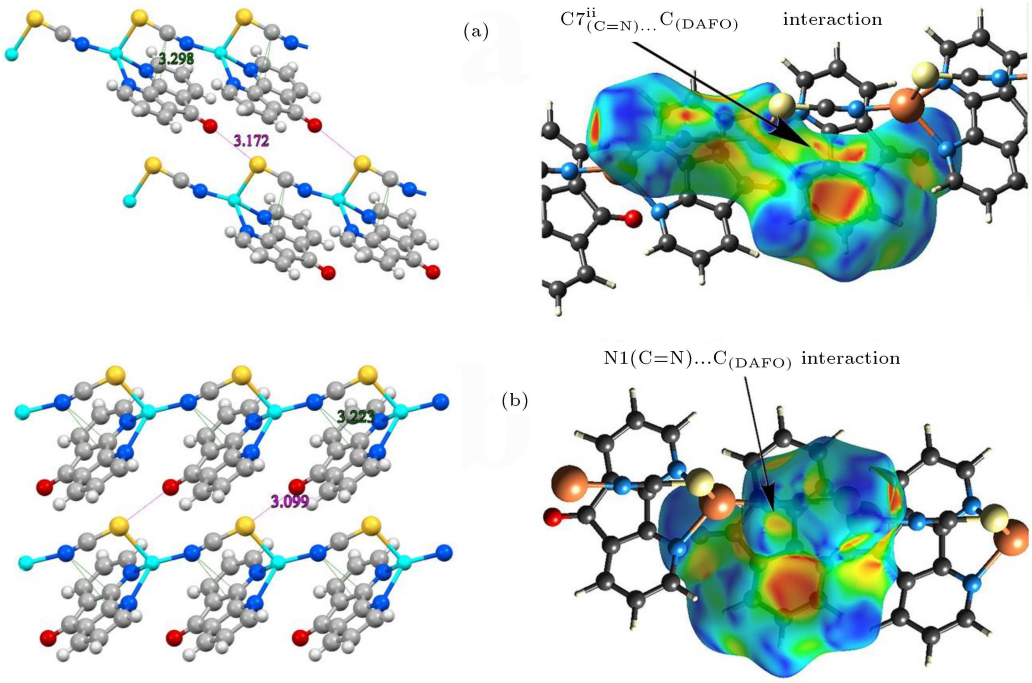

Figure 3. Differences in the 2D polymeric network illustrating inter- and intramolecular interactions with their bond length: (a) $\pi_{C7ii(C=N)...}\pi_{C(DAFO)}$ interaction with bond length and origin in CP1 and (b) $\pi_{N1(C=N)...}\pi_{C(DAFO)}$ interaction with bond length and origin in CP2.

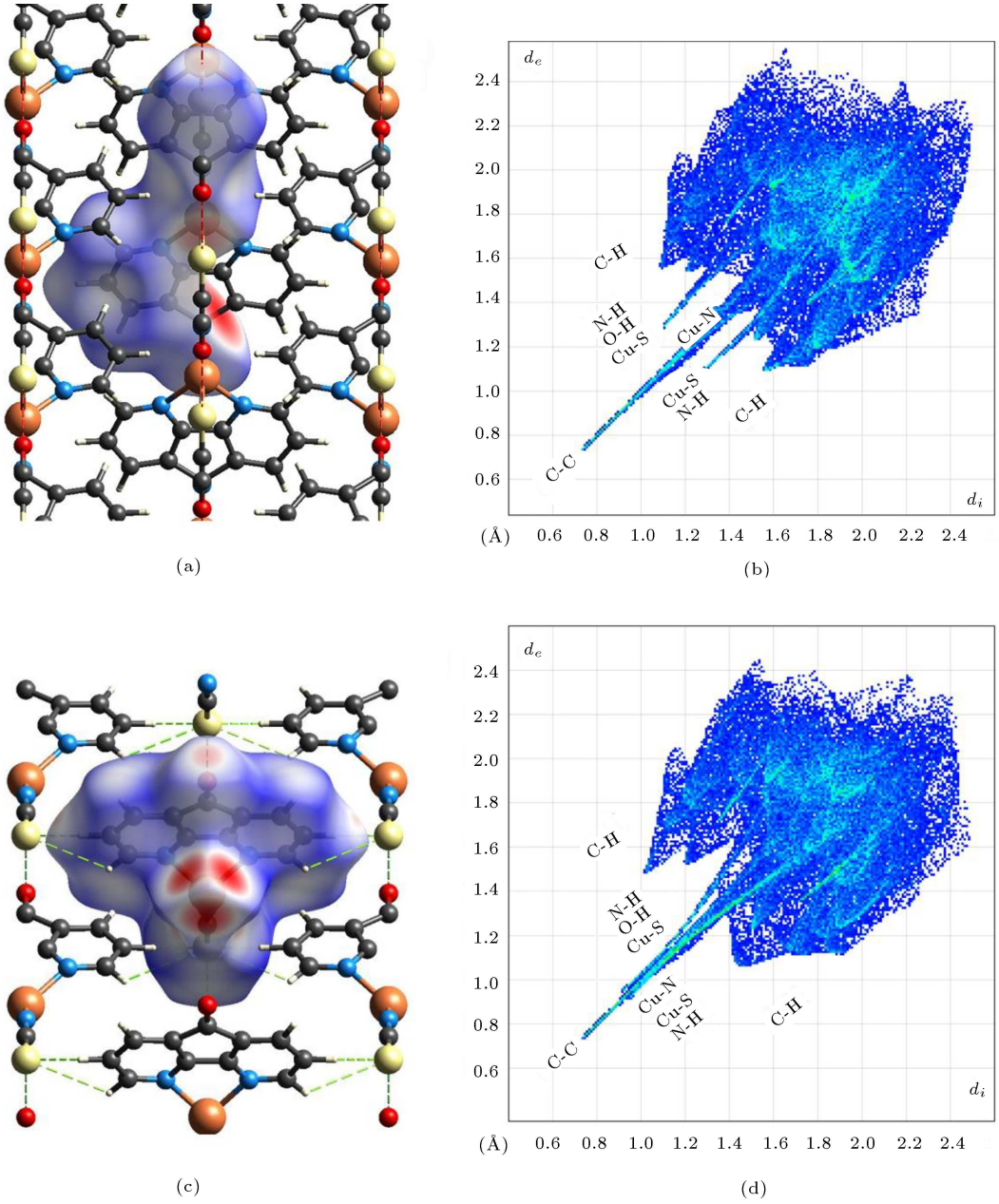

Figure 4. HS analysis and 2D FP mapping for total interactions in (a) CP1 and (b) CP2.

for CP1 are Cu–S (2.394 Å), Cu–N (2.220 Å), $C_{(N\text{-pyridyl moiety})}$–$C_{(5\text{-membered ring})}$ (1.475 Å), and $C_{(ketone\ moiety)}$–$C_{(5\text{-membered ring})}$ (1.475 Å). The $d_e + d_i$ contacts for CP2 are Cu–N^{i} (1.882 Å), Cu–N^{ii} (1.098 Å), $C_{(N\text{-pyridyl moiety})}$–$C_{(5\text{-membered ring})}$ (1.479 Å), and $C_{(ketone\ moiety)}$–$C_{(5\text{-membered ring})}$ (1.497 Å). These dissimilarities result from the determined asymmetric unit of the crystal structure of the CPs.

Based on Figure 6, HS analysis and 2D FP of carbon contacts in both CPs have slight differences. Also, the H–C...H had the dominant contribution.

Figure 7 shows HS analysis and 2D FP mapping of copper contacts in both CPs. It is obvious that there are distinguished differences between Cu–N and Cu–S contact contributions. In CP1, contributions of Cu–N and Cu–S are 3.3% and 4.8% and in CP2 are 11.4% and 0.0%, respectively (see Table 3).

Based on the HS analysis and 2D FP mapping of Figure 8 and Table 3, both CPs have a slight difference in the whole contribution of H-based interactions in the crystal packing system.

With regard to the information given in Table 3, contact contributions of C–N, Cu–N, and Cu–S are

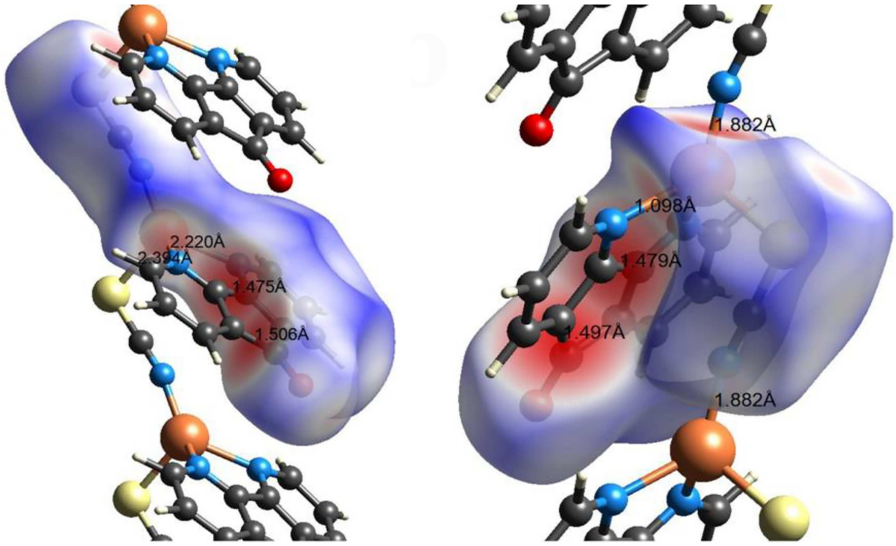

(a) (b)

Figure 5. $d_e + d_i$ for close contact (a) CP1 and (b) CP2.

Table 3. Contact interactions (%) on HS in **CP1** and **CP2**.

Contact type (inside/outside)	CP1	CP2
C–C	8.3	8.2
C–O	3.4	3.5
C–N	8.4	3.3
C–S	4.0	4.0
C–H...C	18.9	19.9
H...H	9.7	8.8
O...H	8.0	8.4
N...H	8.6	8.1
S...H	11.0	11.0
S...O	3.2	3.6
N...O	2.4	2.6
N...S	0.7	0.1
Cu–C	2.1	1.7
Cu–S	4.8	0.0
Cu–N	3.3	11.4
Cu–H	3.3	4.3

impressed by the determined asymmetric units in the course of obtaining crystallography data.

3.5. Non-Covalent Interaction-Reduced Density Gradient (NCI-RDG) method

A fundamental computation strategy that enjoys higher accuracy and precision to visualize weak interactions is the NCI-RDG method [35]. Apart from HS, the real-space color RDG isosurface based on electron density was carried out to obtain more quotative information on the impact of inter- and intra-molecular interactions in the crystal structure by analyzing different colored regions. The blue-green-red colored scale of the surfaces is based on $sign(\lambda_2)\rho$ values, which represent strong attractive interactions, weakly attractive overlap, and strong nonbonding, respectively [36]. Eq. (1) shows that the theory rests on the analysis and graphical interpretation of two scalar properties, charge density ρ and its derivatives, namely the λ eigenvalue of its Hessian and its reduced gradient $s(\rho)$. Therefore, where $\nabla\rho$ is the gradient of ρ, the equation is defined as follows:

$$s = \frac{1}{2(3\pi^2)^{1/3}} \frac{|\nabla\rho|}{\rho^{4/3}}. \quad (1)$$

Low RDG and density regions indicate NCIs. We have spikes at $sign(\lambda_2)\rho < 0$ a.u. for the strong interactions such as H-bonds; at $sign(\lambda_2)\rho$ between ± 0.015 a.u. for the weak vdW types; and at $sign(\lambda_2)\rho > 0$ a.u. for the non-bonded interactions like steric repulsion [37]. The considered structures in Figure 9(b) and (c) were cut out directly from the XYZ data. Since dimerization is the prominent feature of crystal packing in the monomeric complexes, the main NCIs are related to the interactions involved in the formation of dimers. Based on Figure 9(a), there is a more robust repulsion in a five-membered ring than in a six-membered ring in the CP1 crystal structure, which can be understood from one dark red elliptical slab at the center of each six-membered ring and two dark red elliptical slabs at the center of the five-membered ring (Figure 9(b)). The spikes that appeared at 0.05 a.u. belong to the pyridine ring closure. These spikes shift to lower values (less repulsion) in the whole dimeric units of complexes. It can be explained by the effect of metal ion in the charge redistribution as well as the electrostatic interaction between atoms within the rings. In Figure 9(a), the blue region is a slender band at $-0.06 <$

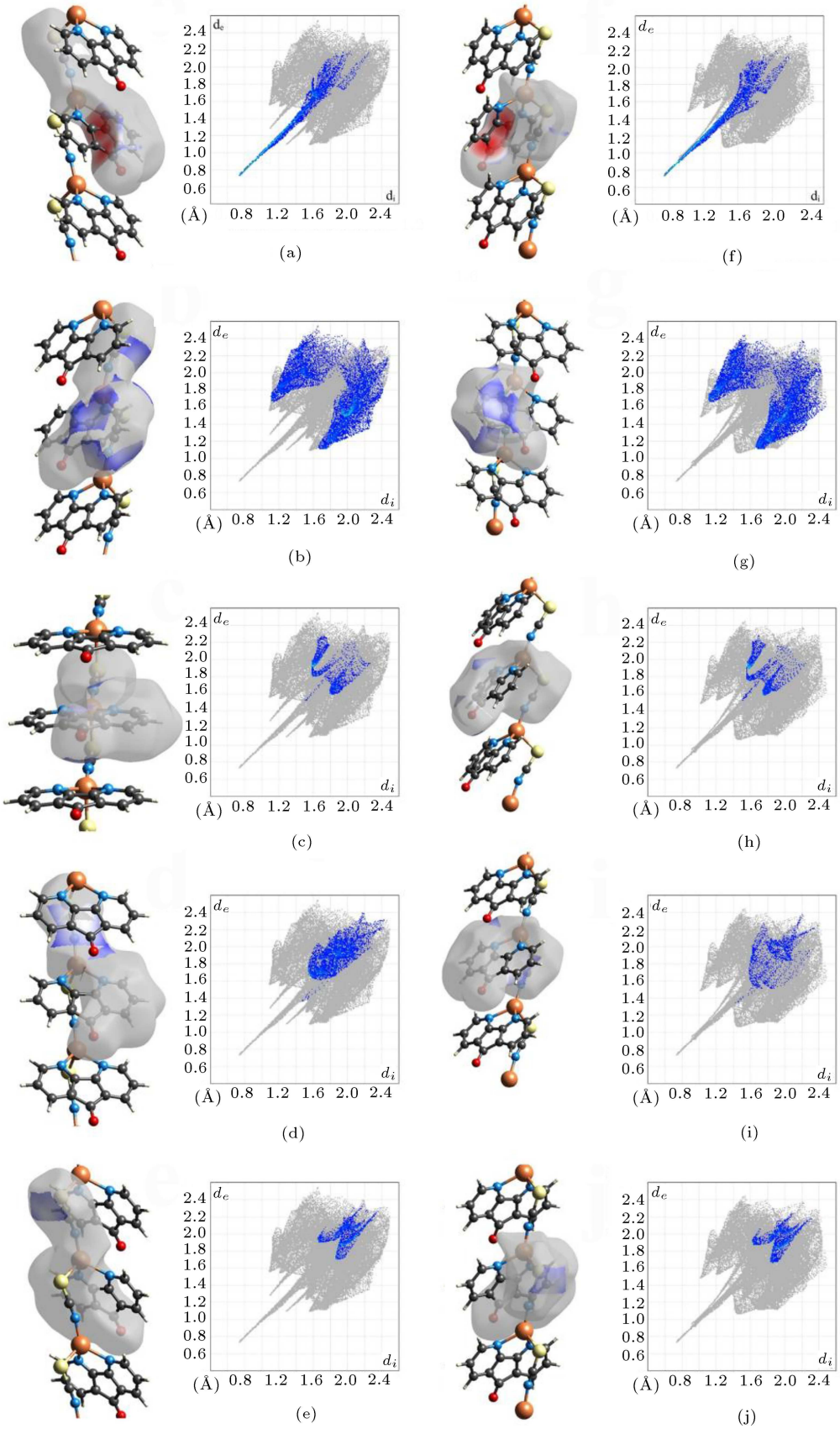

Figure 6. HS analysis and 2D FP mapping of (a) C–C, (b) H–C...H, (c) C–O, (d) C–N, (e) C–S for CP1; and (f) C–C, (g) H–C...H, (h) C–O, (i) C–N, and (j) C–S for CP2.

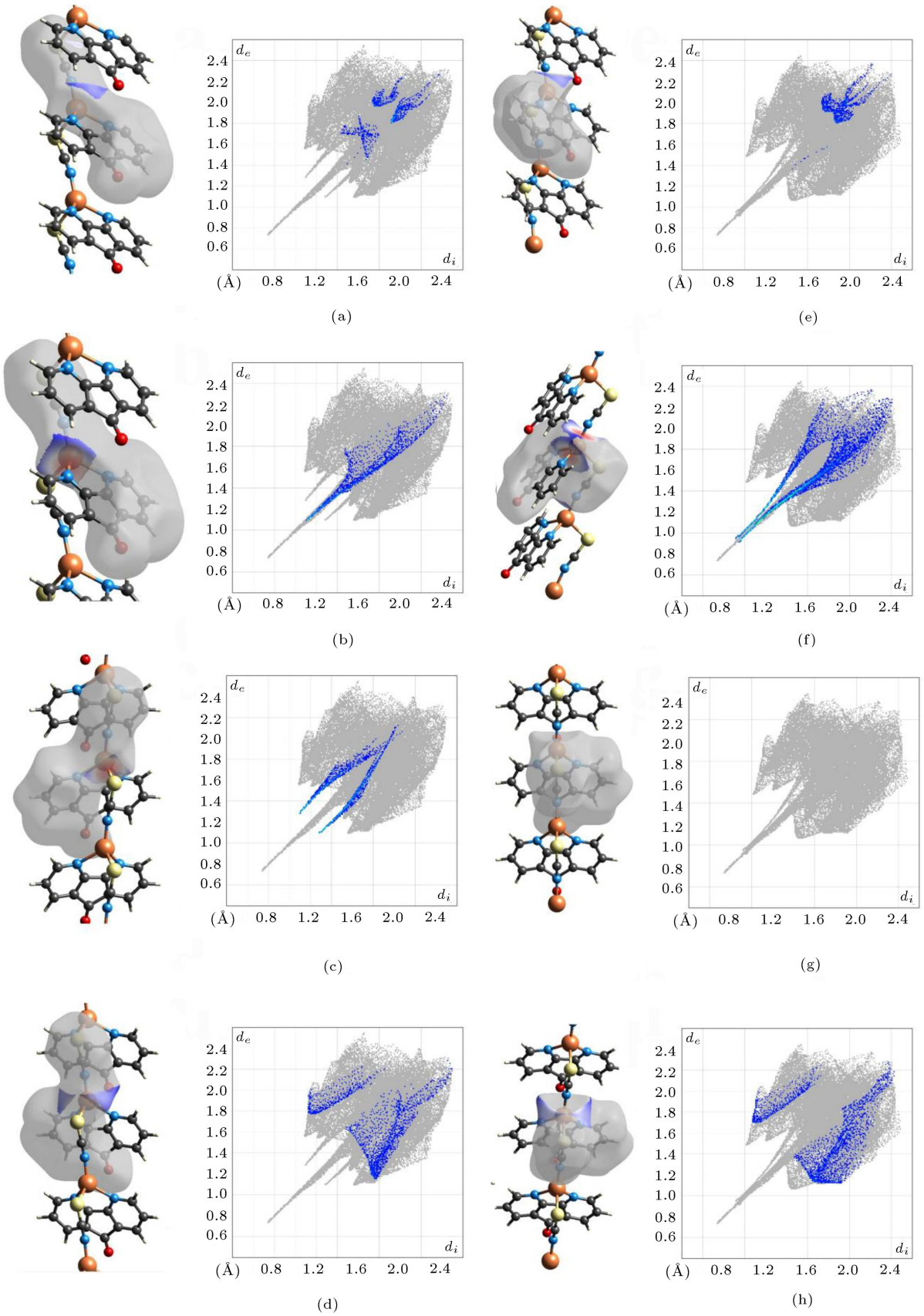

Figure 7. HS analysis and 2D FP mapping of (a) Cu–C, (b) Cu–N, (c) Cu–S, (d) Cu–H for CP1; and (e) Cu–C, (f) Cu–N, (g) Cu–S, and (h) Cu–H for CP2.

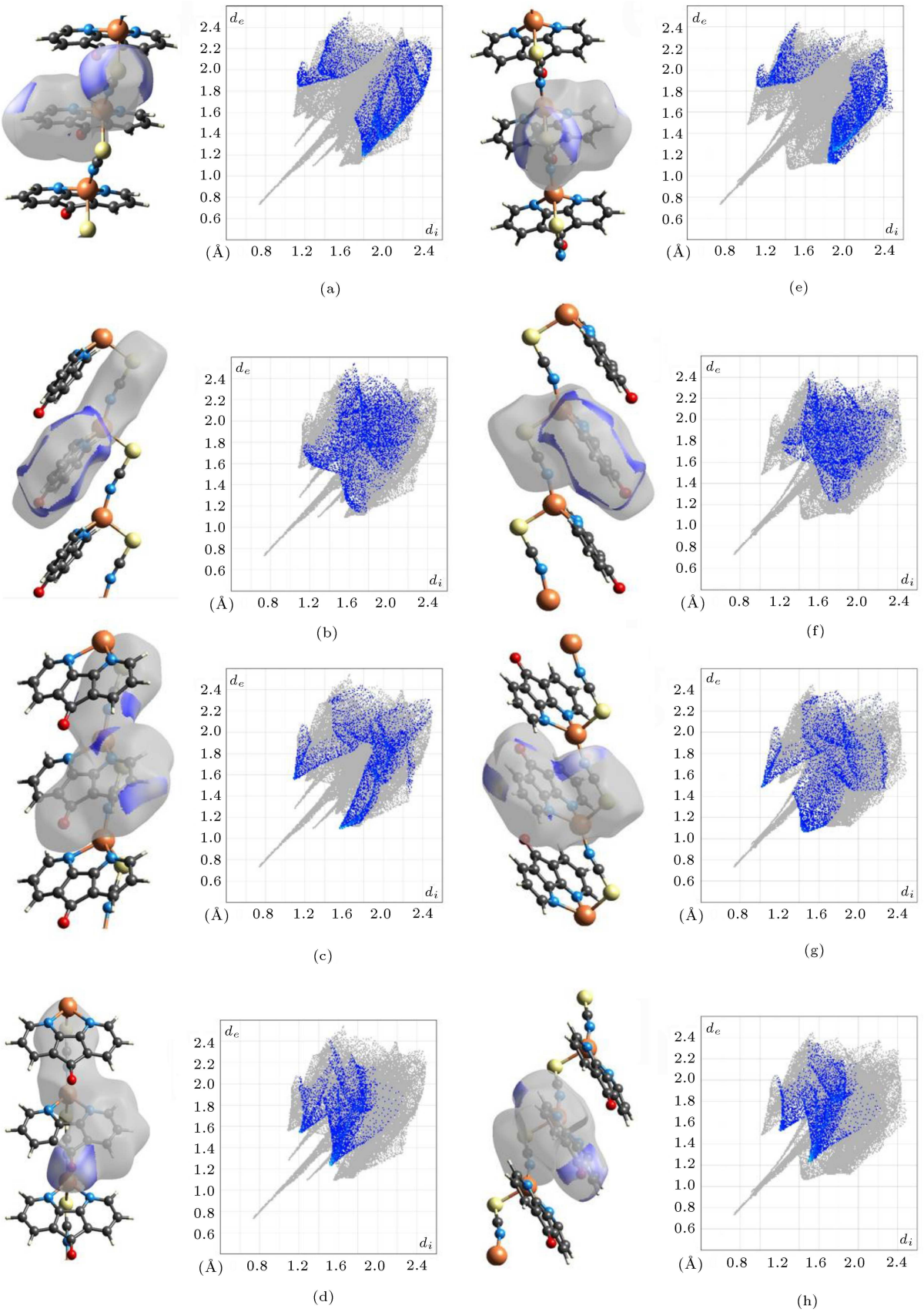

Figure 8. HS analysis and 2D FP mapping of (a) S...H, (b) H...H, (c) N...H, (d) O...H for CP1; and (e) S...H, (f) H...H, (g) N...H, and (h) O...H for CP2.

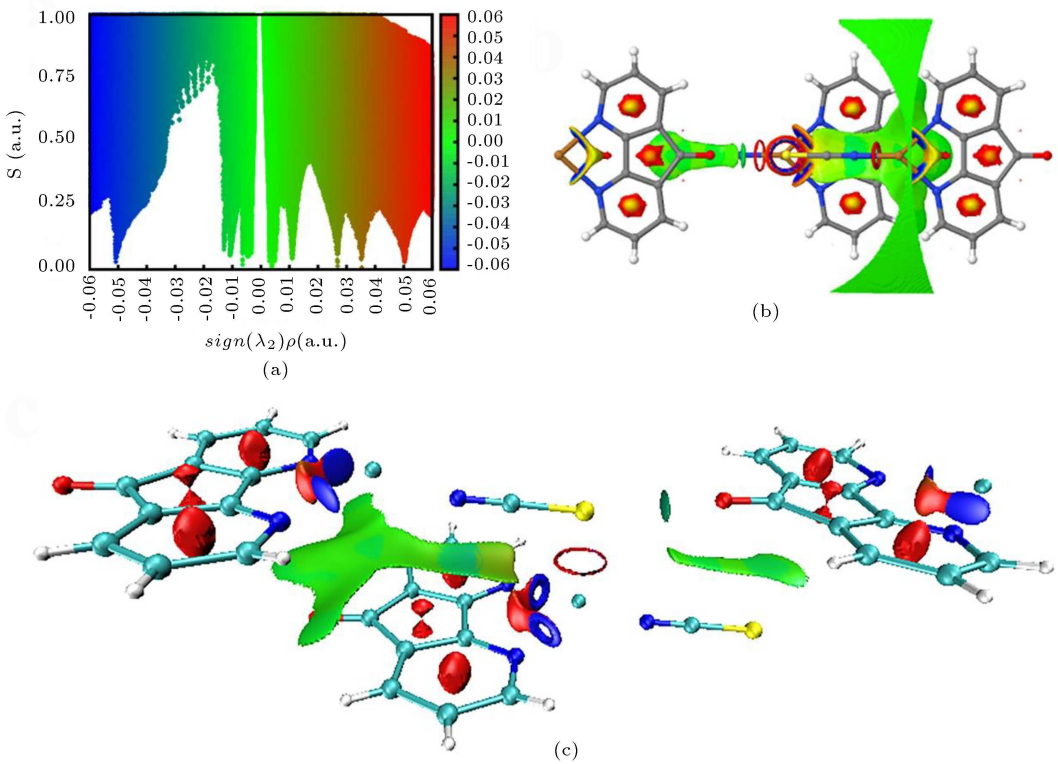

Figure 9. (a) RDG map and NCI plot of gradient isosurface of CP1: (a) scatter graph, (b,c) NCI.

$sign(\lambda_2)\rho < -0.04$ a.u., which indicates that there are strong intermolecular interactions, such as hydrogen bonds in CP1. When $-0.03 < sign(\lambda_2)\rho < +0.03$ a.u., there is a large green region that points to the weak intermolecular interactions and indicates the vdW interactions with lower electron densities [38].

It appears that weak intermolecular vdW interactions play the main role in the crystal packing system. The visual inspection of the isosurfaces in the standard coloring scheme revealed that the CH...X (X=N, S) interaction is likely a hydrogen bond, hence being either directional and specific or vdW. Another appealing feature of the solid-state structure of CP1 is the presence of the lesser-known intermolecular S...O and S...π interactions [39]. NCI-RDG computation plainly implies the notable contribution of these interactions to retaining favorable packing interactions in the complex.

3.6. Synthesis of CuO NPs via solid-state thermal decomposition of CP1

The TEM image and the histogram of the particle size distribution extracted from the image in Figure 10(a) and (b) show the average particle size of ~ 12 nm. The monoclinic phase of as-synthesized CuO NPs based on the Joint Committee on Powder Diffraction Standard (JCPD) number 05–0661 can be extracted from the analysis of assigned crystal planes (Bragg reflection) of strong peaks (Figure 10(c)). In the present work, diffraction patterns at $2\theta = 32.50°$, $35.20°$, $38.30°$, $46.20°$, $48.40°$, $53.15°$, $58.40°$, $61.10°$, $65.60°$, $66.70°$, $72.20°$, $75.10°$ were assigned to the reflection lines of the CuO NPs [40,41]. Since the X-Ray Diffraction (XRD) pattern exhibited no additional peaks, the CuO NPs were highly purified. The crystal size of CuO NPs was calculated from the highest peak at $2\theta = 35.20°$ (111) using the Debye-Scherrer formula and was 12.85 nm. The particle size distribution histogram and the Powder X-Ray Diffraction (PXRD) pattern were quite in agreement. Figure 10(d) shows the fluorescence spectrum of CuO NPs and by applying an excitation wavelength of $\lambda_{ex} = 355$ nm in the ethanol solvent, the fluorescence spectrum at a wavelength of $\lambda_{em} = 462$ nm was recorded [42]. Figure 10(e) shows a relatively wide absorption peak at 307 nm in the visible UV spectrum of CuO NPs. According to Figure 10(f), the band gap energy was calculated at 3.72 eV using the Tauc equation, being higher than CuO in the bulk state (~ 2.1 eV). Figure 10(d) shows a relatively wide absorption peak at 295 nm in the UV-vis spectrum of as-prepared CuO NPs. CuO NPs show smaller particle sizes as E_g increases due to the quantum confinement effect [20,43]. The NPs have a smaller size than the previously synthesized methods [41–43].

4. Conclusion

The hydrothermal reaction condition facilitated producing amazing Coordination Polymers (CPs) such

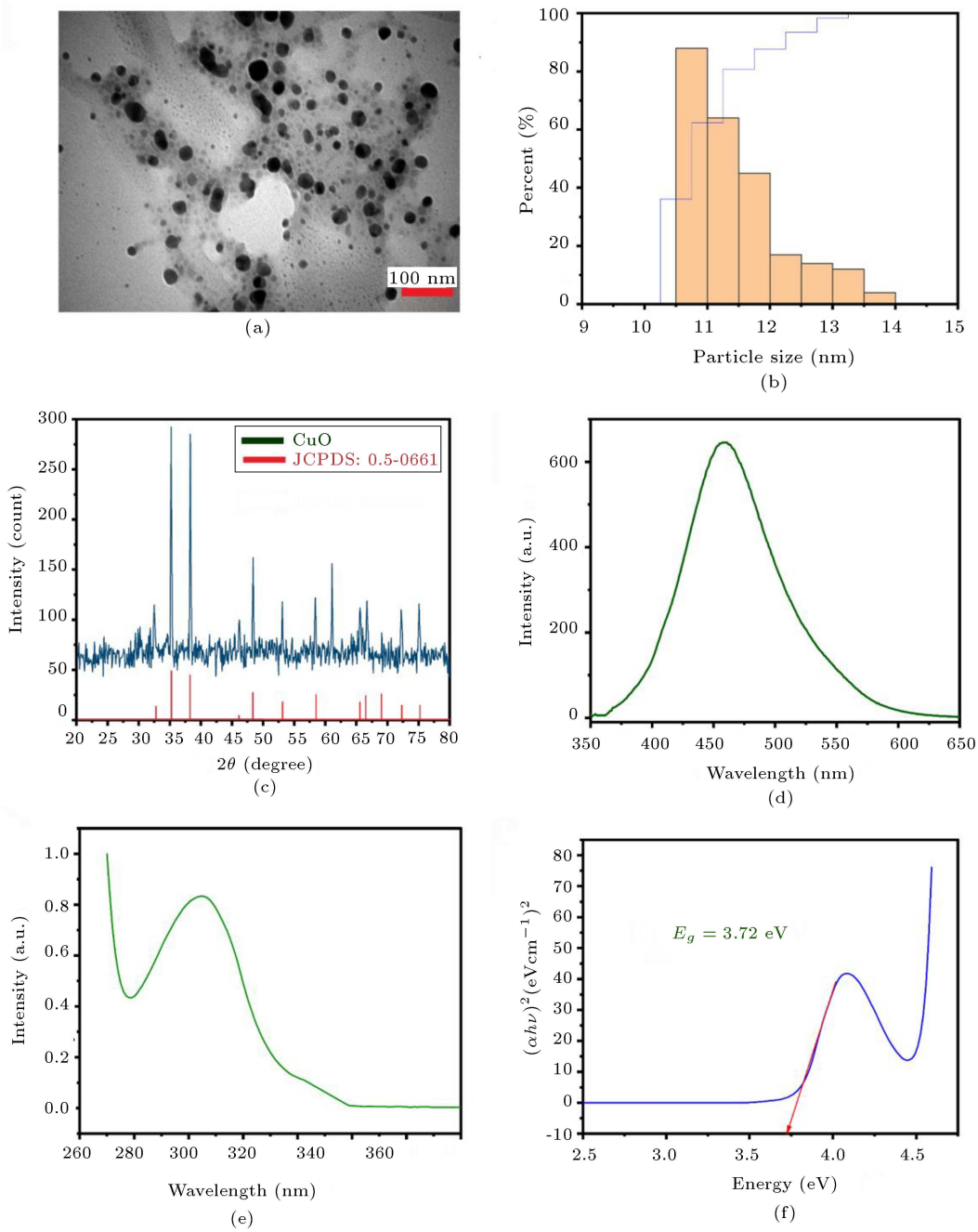

Figure 10. (a) TEM images, (b) Histogram of particle size distribution based on TEM images, (c) PXRD pattern, (d) Florescent spectrum, (e) UV-vis spectrum, and (f) Bandgap energy based on the UV-vis spectrum of as-prepared CuO NPs.

that normal mixing of solutions of ligands and metal salts cannot normally generate them. In our reaction condition, the probable role of copper salt was the Lewis acid catalyst. It produced 2H-tetrazole-5-ammoniumthiolate (Cu-intermediate) following the addition of azide to thiocyanate in ethanol. Although the role of Cu in this reaction remains unclear, the characterization of Cu-intermediate can be an important clue to the role of Cu in such types of reactions. This may broaden our horizon of view on the synthesis of tailor-made and inspiring copper-based CPs. The use of common and cheap metal salt and solvent as well as exact moles of initial reagents make our reaction condition easy and cost-effective. The S...O intermolecular chalcogen bond length and origin of $\pi-\pi$ interaction of SCN^- group with 4,5-Diazafluoren-9-one (DAFO) carbons were influenced by the crystallographic temperature. Results of Ultraviolet-visible (UV-vis) and Fourier Transform Infrared (FT-IR) spectra clarified the bonds and crystal structure of our

CP1. Based on the calculated value of bandgap energy (E_g = 5.63 eV), the result emphasized that CP1 was an ultrawide-bandgap semiconductor material. Bond lengths and angles in the crystal environment (especially, in the geometry center of metal ion) of a coordination compound were affected by the crystallography temperature. The results of our computer study on the Hirshfeld surface analysis and 2D fingerprint plots of both CPs revealed the importance of determining appropriate asymmetric unit in the process of gathering crystallography data. Based on the Non-Covalent Interaction-Reduced Density Gradient (NCI-RDG) and Hirshfeld surface analyses, there are weak interactions, hydrogen bonds, van der Waals (vdW) interactions, and steric effects in the crystal structure of CP1. The polarized aromatic systems of benzene and pyridine ring established $\pi...\pi$ stacking interactions and the presence of the lesser-known intermolecular S...O and S...π interactions in CP1 crystal structure had a significant role in governing the supramolecular assembly of CP1. CP1 single crystals were amenable precursors for copper oxide (CuO) nanoparticles at 750°C in the solid-state thermal decomposition process. The nanoparticles with particle size ∼12 nm were quite small compared with the previously synthesized methods.

Supplementary material

The supplementary material contains supplementary crystallographic data for our coordination polymer of $[Cu(bpdc)(H_2O)2]_n$ (CP1).

Acknowledgements

The authors would like to thank Dr. Julia Contreras-Garcia and Dr. Trinidad Novoa for their expert insight and support in performing NCI-RDG analyses. Unfortunately, given the similarity between the crystal structure of our coordination polymer (CP1) and that synthesized by Kulkarni et al. (CP2), Cambridge Crystallographic Data Centre did not accept our deposit and refused to grant us a CCDC number for our CIF file.

References

1. Kleemiss, F., Dolomanov, O.V., Bodensteiner, M., et al. "Accurate crystal structures and chemical properties from NoSpherA2", *Chem. Sci.*, **12**(5), pp. 1675–1692 (2021).
2. Chen, L.-Q. and Gu, Y., *27 - Computational Metallurgy*, in: D.E. Laughlin, K. Hono (Eds.), Physical Metallurgy (Fifth Edition), Elsevier, Oxford, pp. 2807–2835 (2014).
3. Rutherford, J.S., *Crystal Structure*, in: F. Bassani, G.L. Liedl, P. Wyder (Eds.), *Encyclopedia of Condensed Matter Physics*, Elsevier, Oxford, pp. 289–294 (2005).
4. Ludescher, L., Dirin, D.N., Kovalenko, M.V., et al. "Impact of crystal structure and particles shape on the photoluminescence intensity of CdSe/CdS core/shell nanocrystals", *Front. Chem.*, **6**, pp. 1–11 (2019).
5. Müller, P.C., Ertural, C., Hempelmann, J., et al. "Crystal orbital bond index: Covalent bond orders in solids", *J. Phys. Chem. C*, **125**(14), pp. 7959–7970 (2021).
6. Hughes, S.E., *Chapter 4 - Materials and Their Weldability*, in: S.E. Hughes (Ed.), A Quick Guide to Welding and Weld Inspection, Woodhead Publishing, pp. 36–48 (2009).
7. Purushottam Raj Purohit, R.R.P., Arya, A., Bojjawar, G., et al. "Revealing the role of microstructure architecture on strength and ductility of Ni microwires by in-situ synchrotron X-ray diffraction", *Sci. Rep.*, **9**(1), p. 79 (2019).
8. Saadatian, M.H., Shahverdizadeh, G.H., Babazadeh, M., et al. "The effect of ultrasonic irradiation power and initial concentration on the particle size of nano copper(II) coordination polymer: Precursors for preparation of CuO nanostructures", *J. Polym. Res.*, **29**(2), p. 57 (2022).
9. Sun, Y., Xing, D.-J., Wei, J.-J., et al. "A new Cu(II)-based coordination polymer: application values on liver cancer through down-regulating relative expression of miRNA9", *Polym. Bull.*, **80**(1), pp. 607–619 (2023).
10. Tourani, H., Naimi-Jamal, M.R., Panahi, L., et al. "Nanoporous metal-organic framework Cu2(BDC)2(DABCO) as an efficient heterogeneous catalyst for one-pot facile synthesis of 1,2,3-triazole derivatives in ethanol: Evaluating antimicrobial activity of the novel derivatives", *Scientia Iranica*, **26**(3), pp. 1485–1496 (2019).
11. Hassanein, K., Cappuccino, C.P., Amo-Ochoa, P., et al. "Multifunctional coordination polymers based on copper(I) and mercaptonicotinic ligands: synthesis, and structural, optical and electrical characterization", *Dalton Trans.*, **49**(30), pp. 10545–10553 (2020).
12. Siddiqui, S.A., Prado-Roller, A., and Shiozawa, H. "Room temperature synthesis of a luminescent crystalline Cu–BTC coordination polymer and metal-organic framework", *Mater. Adv.*, **3**(1), pp. 224–231 (2022).
13. Bagherzadeh, M., Mahmoudi, H., Amini, M., et al. "SBA-15-supported copper(II) complex: An efficient heterogeneous catalyst for azide-alkyne cycloaddition in water", *Scientia Iranica*, **25**(3), pp. 1335–1343 (2018).
14. Moraes, L.C., de Souza, G.P., Fajardo, H.V., et al. "1D coordination polymer based on copper(II)-containing tetrameric 1,2,3-triazole ligand from click chemistry:

Magnetic and catalytic properties", *Inorganica Chim. Acta*, **489**, pp. 93–99 (2019).

15. Najafi, M., Abbasi, A., and Masteri-Farahani, M. "Preparation of MoO_3/$CuMoO_4$ nanoparticles as selective catalyst for olefin epoxidation", *Scientia Iranica*, **24**(3), pp. 1203–1208 (2017).
16. Etefagh, R., Rozati, S.M., Azhir, E., et al. "Synthesis and antimicrobial properties of ZnO/PVA, CuO/PVA, and TiO_2/PVA nanocomposites", *Scientia Iranica*, **24**(3), pp. 1717–1723 (2017).
17. Xiong, R.G., Xue, X., Zhao, H., et al. "Novel, acentric metal-organic coordination polymers from hydrothermal reactions involving in situ ligand synthesis", *Angew Chem. Int. Ed. Engl.*, **41**(20), pp. 3800–3 (2002).
18. Liu, J.-C., Huang, J.-S., and You, X.-Z. "Different oxidation states of copper(I, I/II, II) thiocyanate complexes containing 1,2,4-triazole as a bridging ligand: Syntheses, crystal structures, and magnetic properties of 2-D polymer CuI(admtrz)SCN, linear trinuclear $[Cu^{I}_{2}Cu^{II}(admtrz)_6(SCN)_2](ClO_4)_2$, and triangular trinuclear $[Cu^{II}_{3}(admtrz)_4(SCN)_3(\mu_3\text{-}OH)(H_2O)](ClO_4)_2.H_2O$ (admtrz = 4-Amino-3,5-dimethyl-1,2,4-triazole)", *Inorg. Chem.*, **42**(1) pp. 235–243 (2003).
19. Kulkarni, P., Padhye, S., Sinn, E., et al. "Comparative studies on copper(I) complexes: synthesis, X-ray crystallography and electrochemical properties of [CuI(dafone)nX] complexes (dafone=4,5-diaza-fluoren-9-one, X=Br, I, SCN)", *Inorganica Chim. Acta*, **332**(1), pp. 167–175 (2002).
20. Ramezani, B., Hossein Shahverdizadeh, G., Edjlali, L., et al. "Sonochemical synthesis of differently-sized nanoparticles of a silver(I) compound: An optical, anticancer, and thermal activity evaluation study", *Chemistry Select*, **5**(42), pp. 13081–13090 (2020).
21. Dolomanov, O.V., Bourhis, L.J., Gildea, R.J., et al. "OLEX2: a complete structure solution, refinement and analysis program", *J. App. Crystallogr.*, **42**(2), pp. 339–341 (2009).
22. Sheldrick, G. "Crystal structure refinement with SHELXL", *Acta Crystallogr. C*, **71**(1), pp. 3–8 (2015).
23. Demko, Z.P. and Sharpless, K.B. "Preparation of 5-substituted 1H-tetrazoles from nitriles in water", *J. Org. Chem.*, **66**(24), pp. 7945–7950 (2001).
24. Dyga, M., Hayrapetyan, D., Rit, R.K., et al. "Electrochemical ipso-thiocyanation of arylboron compounds", *Adv. Synth. Catal.*, **361**(15), pp. 3548–3553 (2019).
25. Jazdzewski, B.A., Holland, P.L., Pink, M., et al. "Three-coordinate copper(II)-phenolate complexes", *Inorg. Chem.*, **40**(24), pp. 6097–6107 (2001).
26. Katari, M., Payen de la Garanderie, E., Nicol, E., et al. "Combining gas phase electron capture and IRMPD action spectroscopy to probe the electronic structure of a metastable reduced organometallic complex containing a non-innocent ligand", *Phys. Chem. Chem. Phys.*, **17**(39), pp. 25689–25692 (2015).
27. Mohamed, G.G. and El-Gamel, N.E.A. "Synthesis, investigation and spectroscopic characterization of piroxicam ternary complexes of Fe(II), Fe(III), Co(II), Ni(II), Cu(II) and Zn(II) with glycine and dl-phenylalanine", *Spectrochim. Acta A Mol. Biomol. Spectrosc.*, **60**(13), pp. 3141–3154 (2004).
28. Gao, S., Fan, R.-Q., Qiang, L.-S., et al. "Effects of solvents and temperature on the luminescence properties of Cd-isonicotinic acid frameworks based on mono-, bi-, and trinuclear cluster units", *CrystEngComm*, **16**(6), pp. 1113–1125 (2014).
29. Pascoe, D.J., Ling, K.B., and Cockroft, S.L. "The origin of chalcogen-bonding interactions", *J. Am. Chem. Soc.*, **139**(42), pp. 15160–15167 (2017).
30. Liu, L., Sun, Y., Wei, S., et al. "Solvent effect on the absorption and fluorescence of ergone: Determination of ground and excited state dipole moments", *Spectrochim. Acta A Mol. Biomol. Spectrosc.*, **86**, pp. 120–123 (2012).
31. Tsao, J.Y., Chowdhury, S., Hollis, M.A., et al. "Ultrawide-bandgap semiconductors: Research opportunities and challenges", *Adv. Electron. Mater*, **4**(1), 1600501 (2018).
32. Batsanov, A.S., *X-ray Diffraction, Small Molecule Applications*, in: J.C. Lindon, G.E. Tranter, D.W. Koppenaal (Eds.), Encyclopedia of Spectroscopy and Spectrometry (Third Edition), Academic Press, Oxford, pp. 656–666 (2017).
33. Akhileshwari, P., Kiran, K.R., Sridhar, M.A., et al. "Synthesis, crystal structure characterization, Hirshfeld surface analysis, and Quantum chemical computations of Ethyl 5-(thiophene-2-carbonyl)thiazole-4-carboxylate", *J. Mol. Struct.*, **1242**, 130747 (2021).
34. Husain, A., Kumar, G., Sood, T., et al. "Synthesis, structural characterization and DFT analysis of an unusual tryptophan copper(II) complex bound via carboxylate monodentate coordination: Tetraaquabis(l-tryptophan) copper(II) picrate", *Inorganica Chim. Acta*, **482**, pp. 324–332 (2018).
35. Laplaza, R., Peccati, F., Boto, C., et al. "NCIPLOT and the analysis of noncovalent interactions using the reduced density gradient", *Wiley Interdiscip. Rev. Comput. Mol. Sci.*, **11**, p. 1497 (2021).
36. Liu, Y., Fan, J., Xue, Z., et al. "Crystal structure and noncovalent interactions of heterocyclic energetic molecules", *Molecules*, **27**, p. 4969 (2022).
37. Contreras-García, J., Johnson, E.R., Keinan, S., et al. "NCIPLOT: A program for plotting noncovalent interaction regions", *J. Chem. Theory Comput.*, **7**, pp. 625–632 (2011).
38. Gholivand, K., Farshadfar, K., Roe, S.M., et al. "Investigation of structure-directing interactions within copper(I) thiocyanate complexes through X-ray analyses and non-covalent interaction (NCI) theoretical approach", *CrystEngComm*, **18**, pp. 7104–7115 (2016).
39. Boto, R.A., Peccati, F., Laplaza, R., et al. "NCIPLOT4: Fast, robust, and quantitative analysis of

noncovalent interactions", *J. Chem. Theory Comput.*, **16**, pp. 4150–4158 (2020).

40. Zheng, L. and Liu, X. "Solution-phase synthesis of CuO hierarchical nanosheets at near-neutral pH and near-room temperature", *Mater. Lett.*, **61**(11), pp. 2222–2226 (2007).
41. Manjari, G., Saran, S., Arun, T., et al. "Catalytic and recyclability properties of phytogenic copper oxide nanoparticles derived from Aglaia elaeagnoidea flower extract", *J. Saudi Chem. Soc.*, **21**(5), pp. 610–618 (2017).
42. Bhunia, A.K. and Saha, S. "CuO nanoparticle-protein bioconjugate: characterization of CuO nanoparticles for the study of the interaction and dynamic of energy transfer with bovine serum albumin", *BioNanoScience*, **10**(1), pp. 89–105 (2020).
43. Dagher, S., Haik, Y., Ayesh, A.I., et al. "Synthesis and optical properties of colloidal CuO nanoparticles", *J. Lumin.*, **151**, pp. 149–154 (2014).

Biographies

Bahman Ramezani was born in Tabriz, Iran in 1985 and received his BSc degree in Applied Chemistry from Payam Noor University of Iran. He graduated with an MSc degree in Organic Chemistry from Islamic Azad University of Tabriz in 2013 under the supervision of Professor Mirza Agha Babazadeh. He completed his PhD in Organic Chemistry from Islamic Azad University, Tabriz branch in 2019 under the supervision of Dr. Gholamhossein Shahverdizadeh. He is interested in the synthesis of inorganic and organic compounds active in cancer therapy. During his PhD, he had a medicinal chemistry research fellowship at Dr. Fatemeh Ramezani's laboratory at Tabriz Drug Research Center.

Gholam Hossein Shahverdizadeh is an Assistant Professor at the University of Granada and a PhD holder in Inorganic Chemistry from the University of Zanjan. He was born in Tabriz, Iran in 1974. He is particularly interested in the nano-inorganic metal-organic compounds and their versatile applications. Now, he is working at Islamic Azad University, Tabriz Branch as an Associate Professor. He has served as a reviewer for different international journals.

Ladan Edjlali was born in Tabriz, Iran in 1960. She received her BSc degree in Applied Chemistry from University of Tabriz, Iran and her MSc degree in Organic Chemistry from University of Tabriz, Tabriz, Iran in 1993 under the supervision of Professor Mirzaei. She completed his PhD degree in 2000 under the supervision of Professor Mirzaei and Professor Golabi. Now, she is working at Islamic Azad University, Tabriz Branch as an Associate Professor. Her research interests include organic synthesis and new methodologies in organic synthesis.

Fatemeh Ramezani was born in Tabriz, Iran in 1981. She received her BSc degree in Laboratory Science from Medical University of Tabriz, Iran and her MSc degree in Clinical Biochemistry from Medical University of Urmia, Urmia, Iran in 2009 under the supervision of Professor Salami. She completed his PhD degree in 2013 from Medical University of Shiraz, Shiraz, Iran in 2009 under the supervision of Professor Mostafavipour and Professor Samadi. Now, she is working at Tabriz Advanced Medical School, Tabriz, Iran as an Associate Professor. Her research interests consist of three major fields of molecular biology, cancer study, and combination therapy.

Mirzaagha Babazadeh is an Associate Professor of Organic Chemistry at the Department of Chemistry at Tabriz Branch, Islamic Azad University, Tabriz, Iran. He was born in Tabriz, Iran in 1973. He received his BSc degree in Applied Chemistry (1996) and his MSc degree in Organic Chemistry from University of Tabriz, Tabriz, Iran (1999) under the supervision of Professor Entezami and Professor Namazi. He completed his PhD degree under the supervision of Professor Safa in University of Tabriz, Tabriz, Iran (2005). His research interests focus on organic synthesis, catalyst, polymer, green chemistry, drug delivery systems, organosilicon compounds, and nanocomposites.